

Additive manufacturing of Ni-based superalloys: The outstanding issues

Moataz M. Attallah, Rachel Jennings, Xiqian Wang, and Luke N. Carter

There is increasing interest in the use of additive manufacturing (AM) for Ni-based superalloys due to their various applications in the aerospace and power-generation sectors. Ni-based superalloys are known to have a complex chemistry, with over a dozen alloying elements in most alloys, enabling them to achieve outstanding high-temperature mechanical performance as well as oxidation resistance when processed using conventional routes (e.g., casting and forging). Nonetheless, this complex chemistry results in the formation of various phases that could affect their processability using AM, resulting in cracking. Furthermore, due to the directional solidification and rapid cooling associated with AM processes, the alloys experience significant anisotropy due to the epitaxially grown microstructure, as well as the residual stresses that can sometimes be difficult to mitigate using thermal postprocessing techniques. This article highlights the outstanding issues in Ni-based superalloys AM processing, with special emphasis on defect formation mechanisms, process optimization, and residual stress development.

Introduction

Nickel-based superalloys constitute an important class within the broader family of superalloys, with Ni as the main alloying element. They possess a combination of outstanding mechanical and physical properties in the temperature range of 540°C–1000°C, notably tensile and creep strength as well as resistance to thermal fatigue and oxidation, making them especially suitable for gas-turbine and jet-engine components.[1] Alloying elements are selectively included to improve their performance. For instance, Ti, Al, and Nb contribute to the formation of precipitation strengthening phases (Ni_3Al (γ') and Ni_3Nb [γ'']), which are formed as coherent fine precipitates following aging. Other elements (e.g., Ta, Ti, Mo, Hf, W, Cr) contribute to the formation of carbides, which assist in grain-size control and resistance to grain-boundary sliding at high temperatures. Other elements (e.g., Al, Cr, La, Y, Ce) are added to improve their oxidation and corrosion resistance, which is essential to the aforementioned applications.[1,2]

Generally, Inconel 718 (also called Alloy 718) has been the workhorse of the aero-engine sector, due to its combination of good weldability, forgeability, and strength up to 650°C at a reasonable cost.[3] There has been increasing interest in the development of Ni-based superalloys that are capable of higher-temperature performance, in order to increase the turbine entry temperature (TET) of gas turbines (the temperature of combustion byproduct gases entering the turbine section), which manifests in improved thermodynamic efficiency.[4] As a result, newer alloys were developed to achieve this, including CM247LC, RR1000, René 41, Hastelloy-X, Waspaloy, Udimet 720, N18, and Astroloy (**Table I**).[4]

Despite their outstanding high-temperature performance, these alloys have limited weldability due to the presence of a high γ'-fraction (directly linked to the Ti + Al content), which increases the susceptibility of the alloys to cracking during postweld heat treatment (or reheating operations), also known as "strain-age cracking."[5] The alloys also become susceptible to ductility-dip cracking (DDC), which is defined as the drop in ductility at intermediate temperatures (0.4–0.7× the melting point), and is typically associated with the formation of grain-boundary carbides in Ni superalloys.[6] This relationship between alloy chemistry and weld susceptibility is shown in **Figure 1**.[7] This does not include other cracking mechanisms such as liquation and solidification cracking, which could occur during welding of alloys, regardless of the chemistry.

In simple terms, additive manufacturing (AM) can be described as a multilayer/repeated welding process (see the

Moataz M. Attallah, Advanced Materials and Processing Lab, School of Metallurgy and Materials, University of Birmingham, UK; m.m.attallah@bham.ac.uk
Rachel Jennings, Advanced Materials and Processing Lab, School of Metallurgy and Materials, University of Birmingham, UK; REJ024@student.bham.ac.uk
Xiqian Wang, Advanced Materials and Processing Lab, School of Metallurgy and Materials, University of Birmingham, UK; XXW237@student.bham.ac.uk
Luke N. Carter, Advanced Materials and Processing Lab, School of Metallurgy and Materials, University of Birmingham, UK; l.n.carter@bham.ac.uk
doi:10.1557/mrs.2016.211

© 2016 Materials Research Society
https://doi.org/10.1557/mrs.2016.211 Published online by Cambridge University Press

Table I. Chemical compositions (wt%) of selected aerospace Ni-based superalloys.[4]

Alloy	Ni	Cr	Co	Mo	W	Zr	Ti	Al	Fe	C	Other
CM247LC	Bal.	8.0	9.0	0.5	10	0.01	0.7	5.6		0.07	1.4Hf, 3.2Ta, 0.015B
N18	Bal.	11.5	15.5	6.5	–	–	4.3	4.3	–	0.02	0.015B, 0.5Hf
RR1000	Bal.	15.0	18.5	5.0	–	0.06	3.6	3.0	–	0.027	0.015B, 2Ta, 0.5Hf
Astroloy	Bal.	15.0	15.0	5.25	–	0.06	3.5	4.4	<0.3	0.06	0.03B
Udimet 720	Bal.	18.0	14.8	3.0	1.25	0.03	5	2.5	–	0.035	–
René 41	Bal.	19.0	11.0	10.0	–	–	3.1	1.5	<0.3	0.09	0.01B
Waspaloy	Bal.	19.5	13.5	4.3	–	0.09	3.0	1.4	2.0	0.07	0.06B

introductory article in this issue). As such, AM is susceptible to the formation of weld-cracking defects. The processes are associated with rapid cooling rates that were reported to be as high as 10^6 K/s.[8] This results in the formation of significant residual stresses as well as an epitaxially grown microstructure, with both resulting in structural integrity issues and anisotropy in mechanical properties. Process optimization for AM techniques, regardless of the type (e.g., selective laser melting [SLM], electron-beam selective melting, or direct energy deposition [DED] methods) has thus far been performed from an engineering perspective, due to a lack of fundamental understanding of the thermal impact of the process on the microstructure. This article aims to overview the outstanding issues in Ni superalloy AM, highlighting key challenges and current approaches for their mitigation, as well as the potential of AM for "tailoring" the material microstructure.

Residual stress

Residual stress is defined as stationary stress at equilibrium within a material.[9,10] It could arise from mismatches between components, areas within a body, or phases.[9,11] Multiscale residual stresses are determined by their characteristic length: Type I macro-stresses vary over the dimensions of the component; Type II micro-stresses span grain dimensions; Type III form at the atomic scale.[9,11,12] Residual stress introduced by AM during the layer-by-layer processing is known to be complex and large.[12,13] It is attributed to the large spatiotemporal thermal gradients from localized rapid heating and fast cooling during processing.[14] In general, the presence of residual stress within AM parts (mainly arising close to the surface) is undesirable, especially tensile residual stress, as it reduces the effective fatigue and tensile properties and may distort the final geometry[12,14,15] and induce cracks.[12,13,16] When the residual stress overcomes the yield strength of the material, it causes distortion. A large amount of effort has been invested in the control and reduction of residual stresses in AM.[17–19]

Experimental measurement of residual stress has been carried out by the hole drilling method,[20,21] deflection method,[14,22] x-ray diffraction method,[12,14] contour method,[15,23] and neutron diffraction.[15,23] Numerical simulations have also been developed based on finite element methods (FEM) to understand residual stress development, linking the AM process parameters to the melt pool and temperature gradient on the microscopic scale in order to suggest approaches for the reduction of the residual stress.[22,24–26] On the mesoscopic scale, studies were performed to assess the impact of the thermal field on residual stress development in individual laser paths and build layers.[18,22,27,28] On the macroscopic scale, investigations have been performed to predict the deformation and macrostress.[10,14,17,19,22]

In general, the study of residual stress has been limited to simple geometries, such as thin walls for both AM manufactured samples and models,[14,24,26] due to the high computational costs of using a fully coupled thermomechanical model in large-scale structures. The model results are in good agreement with the experimental measurements.[19,29,30] Longitudinal residual stress, with tensile nature with a parabolic distribution, is found near the top of the samples and tends to increase with the number of deposited layers due to the decreasing thermal gradient.[10,21,29,31–33] Stresses have also been

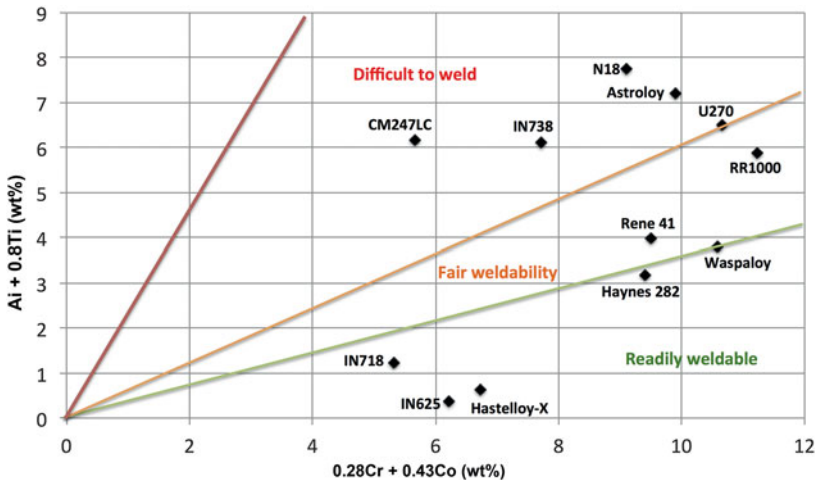


Figure 1. Weldability assessment diagrams for nickel-based superalloys using the chemical composition (wt%) of the γ′-forming elements (Al and Ti) and the carbide-forming elements (Cr and Co). Adapted with permission from Reference 7. © 2006 The Minerals, Metals and Materials Society.

https://doi.org/10.1557/mrs.2016.211 Published online by Cambridge University Press

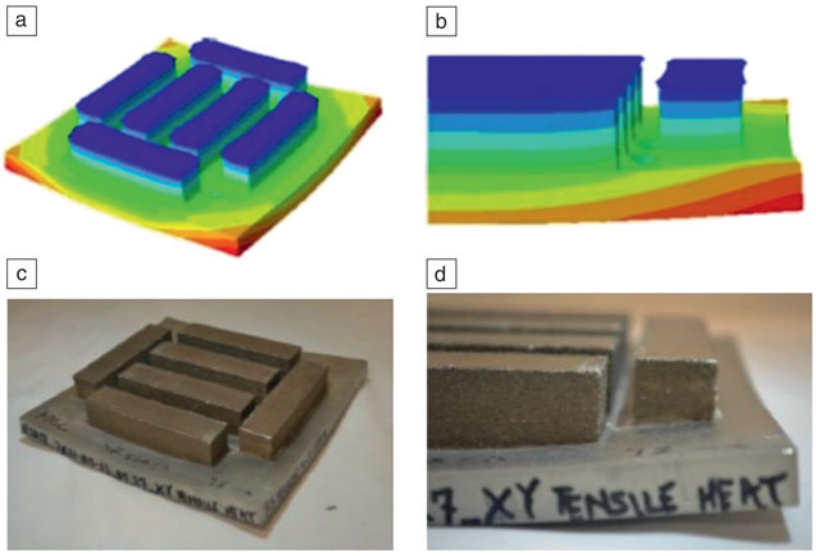


Figure 2. Comparison of warping during electron-beam melting of IN718 in (a–b) simulation results and (c–d) actual components, respectively, showing good agreement. Reprinted with permission from Reference 19. © 2015 Springer.

shown to vary with increasing final build height in thin wall structures, based on the height of the measurement points and the scanning pattern, as longitudinal stresses change from tensile to compressive and may convert to tensile again toward the bottom.[30,34] For the normal direction (building direction), residual stress is compressive in the center of the wall and gradually reverses to tensile toward the edges due to constraints on the baseplate from bending deformation, as shown in **Figure 2**.[12,15,19,23,35] Further modeling has revealed that the presence of high tensile stress near the edge is due to the baseplate constraining the thin wall from bending rather than an increase in the melt pool size.[25]

Theoretical and experimental studies have revealed that both the magnitude and trend of residual stress in AM components are governed by material properties (i.e., small coefficient of thermal expansion, large thermal diffusivity, high thermal conductivity),[14,27,35,36] phase transformation or precipitation,[12,23] geometry of components,[20,25,26,34] the position of specimens,[20] processing parameters,[12,15,26,28] baseplate,[10,19] and scanning pattern.[10,18,22,23,27,34,37] It was found that substrate preheating and insulation could help reduce residual stresses by limiting the thermal gradient between layers and controlling the melt pool, but it may change stress from tension to compression.[18,20,24,26,29,38,39] Shorter laser scanning paths and larger layer thickness lead to less stress due to reduction in the temperature gradient, as shown in **Figure 3**.[10,13,17,22,23,30,37] Alternating the scanning direction also helps lower stresses.[27,30]

In summary, it is difficult to create Ni-based superalloy AM structures with reduced residual stresses (that could be effectively mitigated using postprocess thermal treatments), due to the insufficient flexibility of the AM platforms and the computational cost of predicting scanning strategies and process parameters that will minimize residual stresses. Future AM platforms should employ physics-inspired scanning strategies that will aim to reduce thermal stresses by controlling the thermal gradients in complicated 3D structures. In addition, the hot powder bed systems used in current electron-beam-based platforms should be extended to laser-based systems to mitigate residual stresses *in situ,* similar to electron-beam selective melting systems. Finally, computationally nonintensive codes need to be developed to predict the thermal fields and residual stresses, and potentially control residual stress development on the fly, if these codes can be employed on AM platforms.

Defect formation in AM of Ni-based superalloys: Porosity and cracking

There are two defects commonly associated with AM of Ni-based superalloys—porosity and cracking—and multiple morphologies of these can be identified. The prevalence of defect type is influenced by the AM technique used, the process variables implemented within each technique, and by the composition and morphology of the parent material. Porosity formation in the AM of Ni-based superalloys is predominantly process-induced and does not appear to differ significantly between alloy compositions.[40] It should, however, be noted that residual porosity in the feedstock material (powder) can significantly differ depending on its production route (e.g., gas atomization versus plasma rotating electrode powders), and this porosity can be passed on to the built part.[41] Generally, insufficient melting resulting from low-energy input or poor powder spreading can lead to the formation of large internal voids,[42,43] following a reducing trend in porosity with increase in energy density per unit area. Interestingly, the threshold for consolidation appears to be less dependent on the Ni superalloy type, as seen in **Figure 4**, which shows the transition from lack of fusion to consolidation for several Ni-based superalloys. A similar threshold for consolidation has been seen in direct laser deposition (DLD)-processed Hastelloy-X. In DLD, powders are sprayed from a nozzle and melted *in situ* using a laser.[44]

Another potential cause for defect formation is balling, which occurs when a track of deposited material has reduced

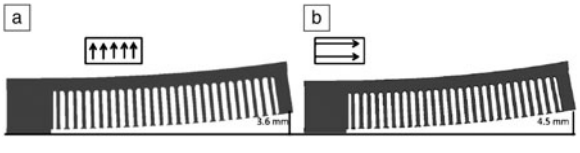


Figure 3. Numerical simulation illustrating varying degrees of deflection in components fabricated using (a) short scanning vector and (b) long scanning vector, showing the influence of the scan strategy on distortion in selective laser melting.[22]

https://doi.org/10.1557/mrs.2016.211 Published online by Cambridge University Press

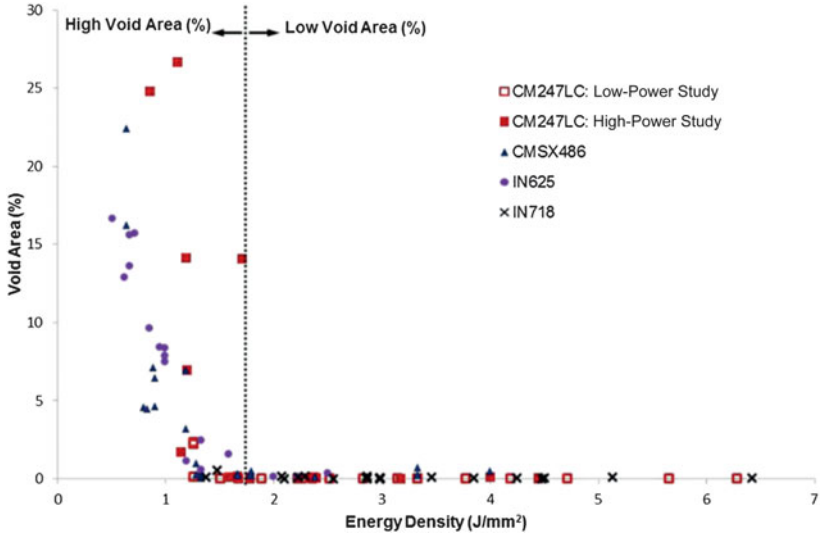


Figure 4. Void area (%) plotted against energy density generated from collated results of five different studies relating to selective laser melting of Ni superalloys IN718, IN625, CM247LC, and CMSX486.[40]

wettability due to an increase in surface tension; a propensity to minimize the surface energy leads to the formation of balls of material, resulting in a rough surface finish and surface porosity. In SLM and DLD of Ni-based superalloys, balling tends to form when low-input energies are used; this can result from an increase in scanning speed[45] or a decrease in laser energy.[46] In addition, the formation of oxides owing to insufficient inert gas shielding can also increase surface tension.[47] However, pores can start to form once the energy density reaches a high enough level to trigger the keyhole-welding mode, where the material exposed to the heat source starts to evaporate, forming a deep keyhole.

Keyhole-induced porosity has been reported to occur in varying geometries according to the spatial level at which it occurs in the keyhole (e.g., the root, middle, or top). While there is some debate as to which morphology comes from where, it is generally agreed that porosity is the result of metal vapor rising out of the keyhole and becoming trapped during keyhole collapse.[48] Keyhole porosity is quite common in Ni-based superalloys due to the large melting range created by having numerous alloying elements. Keyhole porosity has been reported to increase with increasing energy density.[44,49] The heat source (laser or electron beam) profile has been shown to influence keyhole formation, with a broadening of the beam leading to a reduction in keyholing.[49,50]

Four cracking mechanisms can be identified resulting from the AM processing of Ni-based superalloys, including solidification cracking, liquation cracking, DDC, and postweld heat treatment (PWHT) cracking.[51] Rapid cooling during solidification results in the trapping of liquid between already solidified dendrites; when stressed, these weak mushy regions rupture and tear,[51,52] creating jagged solidification cracks. Solidification cracking has been seen to occur when high energy densities are implemented during AM.[51,53,54] Conversely, other work has emerged suggesting that high energy densities actually lead to a reduction in cracking.[43,45] In addition to this, component size has also been shown to affect the onset of solidification cracking, with larger components producing greater thermal gradients and increased solidification cracking.[53] Several studies have recently emerged on the effects of Zr segregation on solidification cracking in IN738LC. It is suggested that Zr films become trapped between dendrite arms near the grain boundaries, embrittling the grain-boundary region; when stressed, cracks form with similar morphology to solidification cracking.[49,55,56]

Other studies point to the impact of the scanning strategy on the formation of solid-state DDC, indicating the role of re-melting and rapid solidification with increasing fraction of high-angle grain boundaries and grain-boundary phases, which leads to the development of DDC when combined with high residual stresses.[57] The welding literature suggests that DDC occurs due to the formation of carbides at grain boundaries,[58] with some reports also suggesting grain-boundary shearing.[59–61] It should be noted that in the latter case, DDC in Ni superalloys always forms along regions of high-angle grain boundaries.[62] Low-melting-point phases resulting from

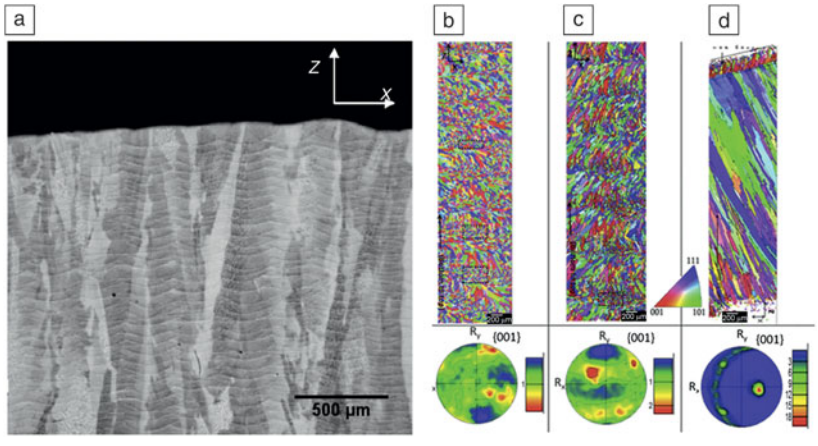


Figure 5. (a) Coarse columnar grains extending several layers along the build direction in selective laser melting-processed Nimonic 263, also showing the fish-scale morphology,[67] and (b–d) electron backscatter diffraction maps for direct laser deposition-processed IN718, showing the impact of the deposition strategy on the grain morphology and texture; (b) unidirectional deposition, (c) bidirectional deposition, and (d) high laser power.[65]

https://doi.org/10.1557/mrs.2016.211 Published online by Cambridge University Press

constitutional undercooling form in grain-boundary regions; when heat is applied, these phases melt and the liquid penetrates the grain boundaries, weakening them and resulting in liquation cracking. Tensile stresses created by contracting material elsewhere pull apart the weakened grain boundaries, forming relatively smooth cracks.[51] Nonetheless, limited studies identified high-energy input during AM as the reason for liquation cracking.[63]

Microstructural anisotropy

AM techniques generally result in a columnar grain structure, with grains extending over several re-melt layers. The rapid solidification, combined with the directionality in heat losses vertically toward the substrate, results in epitaxial growth in either the powder bed or the DED methods,[64,65] see **Figure 5**. Some variability was observed in SLM fabricated structures, whereby the use of a chessboard scanning strategy (in which the laser moves randomly between square islands to evenly distribute the heating) resulted in the formation of nearly equiaxed grains regions embedded within primarily columnar grain regions.[57] A similar variation was also observed in DLD methods, and was attributed to the cooling history of the builds, which can also be manipulated using the build strategy.[66] More importantly, due to the repeated heating nature of the process, the microstructure also shows inhomogeneity on the tens of microns scale, which manifests itself in the "fish-scale" morphology seen in Figure 5a[67] and the inhomogeneity in grain structure or segregation.[68]

The anisotropy in the grain structure is not an issue itself, provided that it can be utilized to tailor a specific mechanical performance similar to the directionality of directionally cast (DS) structures. Nonetheless, this potential has not been fully exploited by the AM user community. Recent work has shown the potential of AM in controlling both the grain size and crystallographic orientation by manipulating the process parameters (Figure 5b–d).

The other challenge associated with the microstructure is the metastable nature of the rapid solidification byproducts in the build. Most Ni-based superalloy AM builds show either considerable levels of interdendritic segregation or other undesirable solidification-induced phases (e.g., Laves phase).[65] As a result, there is always a need for a postprocessing treatment, such as hot isostatic pressing (HIP) to heal the defects caused by the AM processes, often in addition to a solution and aging heat treatment to create the optimum size and fraction of precipitates for high-temperature properties. These postprocessing operations obviously add to the cost of AM processes, making them less attractive.

Mechanical properties

One of the challenges affecting the maturity of AM for Ni superalloys is the lack of sufficient information in the public

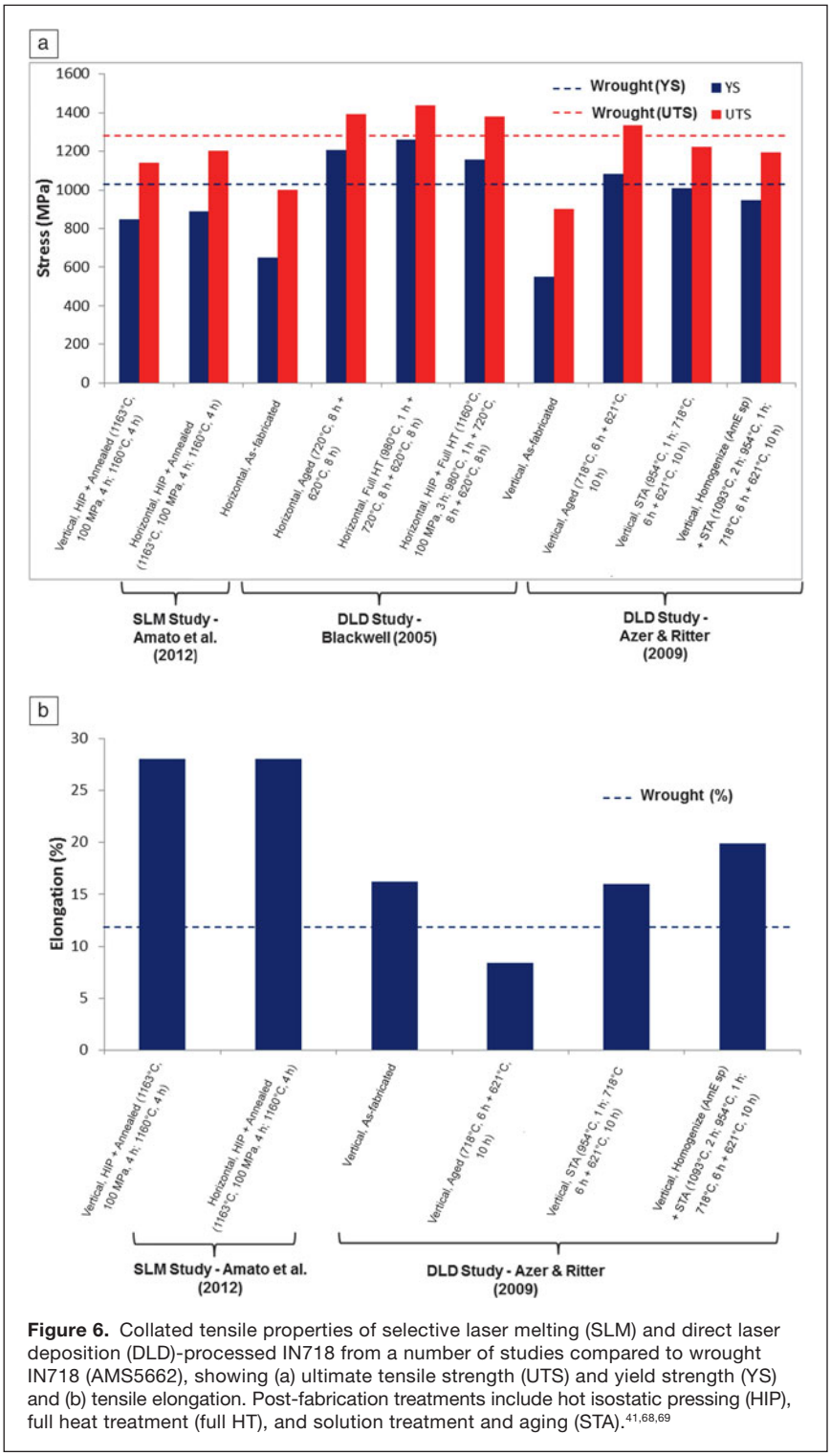


Figure 6. Collated tensile properties of selective laser melting (SLM) and direct laser deposition (DLD)-processed IN718 from a number of studies compared to wrought IN718 (AMS5662), showing (a) ultimate tensile strength (UTS) and yield strength (YS) and (b) tensile elongation. Post-fabrication treatments include hot isostatic pressing (HIP), full heat treatment (full HT), and solution treatment and aging (STA).[41,68,69]

https://doi.org/10.1557/mrs.2016.211 Published online by Cambridge University Press

domain on their high-temperature mechanical performance, notably their creep and high-temperature fatigue performance, due to the testing costs. Furthermore, the available data were generated through various AM platforms, feedstock material characteristics and chemistries, process parameters, scanning strategies, build/sample geometry, and postprocessing treatments, making it difficult to obtain a coherent consensus about the mechanical performance of AM structures.

Figure 6[69] shows the tensile properties of SLM- and DLD-processed IN718, collated from a number of studies. One clear observation is that the as-fabricated properties do not achieve the required performance. Nonetheless, postprocessing, whether or not employing HIP, shows a significant improvement in the tensile properties, especially when a full solution treatment and aging sequence is utilized. Although earlier studies showed strength levels in SLM-processed structures lower than those in wrought material, a recent study[70] showed that strength levels exceeding the wrought condition can be achieved in SLM-processed IN718 once the postprocessing heat treatment is optimized. Nonetheless, heat treatments cannot address the intrinsic anisotropy in the mechanical properties, which usually results in the horizontally built samples slightly overperforming the vertically built samples.

Conclusions

During the last decade, research on AM of Ni superalloys has addressed a number of material and process challenges. Further work is still required to address the residual stress development, microstructure–properties development, and process optimization. This depends on the improvement of flexibility in the AM platforms as well as the development of rapid computational techniques that can simulate the process to maximize the process and product performance.

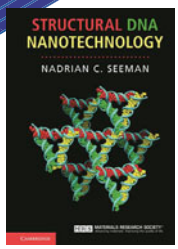
References

1. M.J. Donachie, S.J. Donachie, *Superalloys: A Technical Guide*, 2nd ed. (ASM International, Materials Park, OH, 2002).
2. M. Durand-Charre, *The Microstructure of Superalloys* (Gordon and Breach Science Publishers, Amsterdam, 1997).
3. R. Schafrik, R. Sprague, *Key Eng. Mater.* **380**, 113 (2008).
4. R.C. Reed, *The Superalloys: Fundamentals and Applications* (Cambridge University Press, New York, 2006).
5. M.B. Henderson, D. Arrell, R. Larsson, M. Heobel, G. Marchant, *Sci. Technol. Weld. Joining* **9**, 13 (2004).
6. G.A. Young, T.E. Capobianco, M.A. Penik, B.W. Morris, J.J. McGee, *Weld. J.* **87**, 31 (2008).
7. E.A. Ott, J. Groh, H. Sizek, *Proc. Sixth Int. Special Emphasis Symp. Superalloys 718, 625, 706 and Derivatives*, E.A. Loria, Ed. (The Minerals, Metals and Materials Society, Warrendale, PA, 2006), pp. 35–46.
8. N.J. Harrison, I. Todd, K. Mumtaz, *Acta Mater.* **94**, 59 (2015).
9. P. Withers, H. Bhadeshia, *Mater. Sci. Technol.* **17**, 355 (2001).
10. P. Mercelis, J.-P. Kruth, *Rapid Prototyp. J.* **12**, 254 (2006).
11. P. Withers, H. Bhadeshia, *Mater. Sci. Technol.* **17**, 366 (2001).
12. A. Pinkerton, J. Shackleton, R. Moat, L. Li, P. Withers, M. Preuss, J. Allen, P. Hilton, R. Folwell, *Proc. 24th Int. Congr. Applic. Lasers Electro-optics (ICALEO)* (Laser Institute of America, Orlando, FL, 2005), pp. 601–610.
13. D.D. Gu, W. Meiners, K. Wissenbach, R. Poprawe, *Int. Mater. Rev.* **57**, 133 (2012).
14. B. Vrancken, R. Wauthlé, J.-P. Kruth, J. Van Humbeeck, *Proc. Solid Freeform Fabr. Symp.* (The University of Texas at Austin, Austin, TX, 2013), pp. 1–15.
15. R. Moat, A. Pinkerton, L. Li, P. Withers, M. Preuss, *Mater. Sci. Eng. A* **528**, 2288 (2011).
16. M. Zhong, H. Sun, W. Liu, X. Zhu, J. He, *Scr. Mater.* **53**, 159 (2005).
17. L.L. Parimi, M.M. Attallah, J. Gebelin, R.C. Reed, *Proc. Superalloys 2012*, E.S. Huron, R.C. Reed, M.C. Hardy, M.J. Mills, R.E. Montero, P.D. Portella, J. Telesman, Eds. (Wiley, New York, 2012), pp. 509–519.
18. N. Klingbeil, J. Beuth, R. Chin, C. Amon, *Int. J. Mech. Sci.* **44**, 57 (2002).
19. P. Prabhakar, W. Sames, R. Dehoff, S. Babu, *Addit. Manuf.* **7**, 83 (2015).
20. C. Casavola, S. Campanelli, C. Pappalettere, *J. Strain Anal. Eng. Des.* **44**, 93 (2009).
21. M. Griffith, M. Schlienger, L. Harwell, M. Oliver, M. Baldwin, M. Ensz, M. Essien, J. Brooks, C. Robino, E.J. Smugeresky, *Mater. Des.* **20**, 107 (1999).
22. F. Neugebauer, N. Keller, X. Hongxiao, C. Kober, V. Ploshikhin, *Proc. Fraunhofer Direct Digital Manuf. Conf.* (Fraunhofer Verlag, Stuttgart, Germany, 2014).
23. P. Rangaswamy, M. Griffith, M. Prime, T. Holden, R. Rogge, J. Edwards, R. Sebring, *Mater. Sci. Eng. A* **399**, 72 (2005).
24. A. Vasinonta, J.L. Beuth, M.L. Griffith, *J. Manuf. Sci. Eng.* **123**, 615 (2001).
25. P. Aggarangsi, J.L. Beuth, M. Griffith, *Proc. Solid Freeform Fabr. Symp.* (The University of Texas at Austin, Austin, TX, 2003), pp. 196–207.
26. J. Beuth, N. Klingbeil, *JOM* **53**, 36 (2001).
27. K. Dai, L. Shaw, *Rapid Prototyp. J.* **8**, 270 (2002).
28. L. Wang, S.D. Felicelli, P. Pratt, *Mater. Sci. Eng. A* **496**, 234 (2008).
29. M. Labudovic, D. Hu, R. Kovacevic, *J. Mater. Sci.* **38**, 35 (2003).
30. M.F. Zaeh, G. Branner, *Prod. Eng.* **4**, 35 (2010).
31. R. Moat, A.J. Pinkerton, D.J. Hughes, L. Li, P.J. Withers, M. Preuss, "Stress Distributions in Multilayer Laser Deposited Waspaloy Parts Measured Using Neutron Diffraction, *Proc. 25th Int. Congr. on Applic. Lasers Electro-optics (ICALEO)* (Laser Institute of America, Orlando, FL, 2007).
32. X. Song, M. Xie, F. Hofmann, T. Illston, T. Connolley, C. Reinhard, R. Atwood, L. Connor, M. Drakopoulos, L. Frampton, *Int. J. Mater. Form.* **8**, 245 (2015).
33. A.S.C. D'Oliveira, P.S.C. da Silva, R.M. Vilar, *Surf. Coat. Technol.* **153**, 203 (2002).
34. S. Zekovic, R. Dwivedi, R. Kovacevic, *Proc. Solid Freeform Fabr.* (The University of Texas at Austin, Austin, TX, 2005).
35. N. Shamsaei, A. Yadollahi, L. Bian, S.M. Thompson, *Addit. Manuf.* **8**, 12 (2015).
36. A. Gåård, P. Krakhmalev, J. Bergström, *J. Alloys Compd.* **421**, 166 (2006).
37. A. Nickel, D. Barnett, F. Prinz, *Mater. Sci. Eng. A* **317**, 59 (2001).
38. S. Finnie, W. Cheng, I. Finnie, J.-M. Drezet, M. Gremaud, *J. Eng. Mater. Technol.* **125**, 302 (2003).
39. R.A. Kupkovits, R.W. Neu, *Int. J. Fatigue* **32**, 1330 (2010).
40. L.N. Carter, X. Wang, N. Read, R. Khan, M. Aristizabal, K. Essa, M.M. Attallah, *Mater. Sci. Technol.* **32**, 657 (2015).
41. H. Qi, M. Azer, A. Ritter, *Metall. Mater. Trans. A* **40**, 2410 (2009).
42. L.N. Carter, K. Essa, M.M. Attallah, *Rapid Prototyp. J.* **21**, 423 (2015).
43. M. Ramsperger, R. Singer, C. Körner, *Metall. Mater. Trans. A* **47**, 1469 (2016).
44. F. Wang, X. Wu, D. Clark, *Mater. Sci Technol.* **21**, 344 (2011).
45. Q. Jia, D. Gu, *J. Alloys Compd.* **585**, 713 (2014).
46. K.A. Mumtaz, P. Erasenthiran, N. Hopkinson, *J. Mater. Process. Technol.* **195**, 77 (2008).
47. S. Das, T.P. Fuesting, G. Danyo, L.E. Brown, J.J. Beaman, D.L. Bourell, *Mater. Des.* **21**, 63 (2000).
48. P.S. Wei, S.C. Kou, in *Advances in Multiphase Flow and Heat Transfer*, L. Cheng, Ed. (Bentham Science Publishers, online, 2009), vol. 1, pp. 213–232.
49. M. Cloots, P.J. Uggowitzer, K. Wegener, *Mater. Des.* **89**, 770 (2016).
50. H.E. Helmer, C. Körner, R.F. Singer, *J. Mater. Res.* **29**, 1987 (2014).
51. L. Carter, M. Attallah, R. Reed, *Proc. Superalloys 2012*, E.S. Huron, R.C. Reed, M.C. Hardy, M.J. Mills, R.E Montero, P.D. Portella, J. Telesman, Eds. (Wiley, New York, 2012) pp. 577–586.
52. C. Cross, in *Hot Cracking Phenomena in Welds*, T. Böllinghaus, H. Herold, Eds. (Springer, Berlin, 2005), chap. 1, pp. 3–18.
53. D. Dye, O. Hunziker, R.C. Reed, *Acta Mater.* **49**, 683 (2001).
54. M.T. Rush, P.A. Colegrove, Z. Zhang, D. Broad, *J. Mater. Process. Technol.* **212**, 188 (2012).
55. Y.-L. Tsai, S.-F. Wang, H.-Y. Bor, Y.-F. Hsu, *Mater. Sci. Eng. A* **607**, 294 (2014).
56. D. Heydari, A.S. Fard, A. Bakhshi, J.M. Drezet, *J. Mater. Process. Technol.* **214**, 681 (2013).
57. L.N. Carter, C. Martin, P.J. Withers, M.M. Attallah, *J. Alloys Compd.* **615**, 338 (2014).
58. G. Young, T. Capobianco, M. Penik, B. Morris, J. McGee, *Weld. J.* **87**, 31 (2008).
59. M.L. Collins, J.C. Lippold, *Weld. J.* **82**, 288S (2003).
60. M.R. Collins, A. Ramirez, J.C. Lippold, *Weld. J.* **82** (12), 348S (2003).
61. M. Collins, A. Ramirez, J. Lippold, *Weld. J.* **83**, 39 (2004).
62. J. Lippold, *Welding Metallurgy and Weldability* (Wiley, Hoboken, NJ, 2015).
63. G. Bi, A. Gasser, *Phys. Procedia* **12**, 402 (2011).
64. S. Das, *Adv. Eng. Mater.* **5**, 701 (2003).

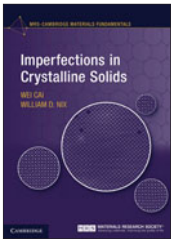
https://doi.org/10.1557/mrs.2016.211 Published online by Cambridge University Press

65. L.L. Parimi, G. Ravi, D. Clark, M.M. Attallah, *Mater. Charact.* **89**, 102 (2014).
66. F. Liu., X. Lin, G.L. Yang, M.H. Song, J. Chen, W.D. Huang, *Opt. Laser Technol.* **43**, 208 (2011).
67. T. Vilaro, C. Colin, J.D. Bartout, L. Naze, M. Sennour, *Mater. Sci. Eng. A* **534**, 446 (2012).
68. K.N. Amato, S.M. Gaytan, L.E. Murr, E. Martinez, P.W. Shindo, J. Hernandez, S. Collins, F. Medina, *Acta Mater.* **60**, 2229 (2012).
69. P.L. Blackwell, *J. Mater. Process. Technol.* **170**, 240 (2005).
70. E. Chlebus, K. Gruber, B. Kuźnicka, J. Kurzac, T. Kurzynowski, *Mater. Sci. Eng. A* **639**, 647 (2015). □

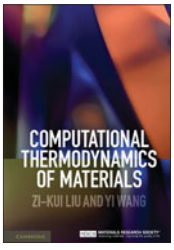
Recent Titles
from the Materials Research Society
and Cambridge University Press
Book Collection



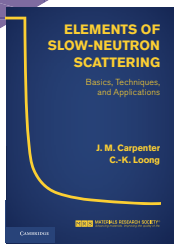
2016 PROSE Award Winner in Biological Science
Structural DNA Nanotechnology
AUTHOR: Nadrian C. Seeman
ISBN: 9780521764483
List Price: $65.00
MRS Member Price: $52.00



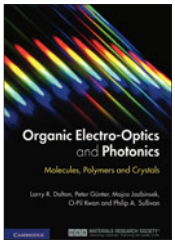
From the new MRS-Cambridge Materials Fundamentals Series
Imperfections in Crystalline Solids
AUTHORS: Wei Cai and William D. Nix
ISBN: 9781107123137
List Price: $65.00
MRS Member Price: $52.00



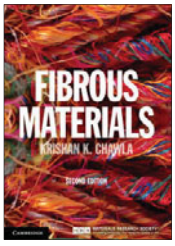
Computational Thermodynamics of Materials
AUTHORS: Zi-Kui Liu and Yi Wang
ISBN: 9780521198967
List Price: $90.00
MRS Member Price: $72.00



Elements of Slow-Neutron Scattering
Basics, Techniques, and Applications
AUTHORS: J.M. Carpenter and C.-K. Loong
ISBN: 9780521857819
List Price: $175.00
MRS Member Price: $140.00



Organic Electro-Optics and Photonics
Molecules, Polymers, and Crystals
AUTHORS: Larry R. Dalton, Peter Günter, Mojca Jazbinsek, O-Pil Kwon and Philip A. Sullivan
ISBN: 9780521449656
List Price: $80.00
MRS Member Price: $64.00



Fibrous Materials
AUTHOR: Krishan K. Chawla
ISBN: 9781107029729
List Price: $110.00
MRS Member Price: $88.00

To learn more about these, and our entire book collection, visit **www.mrs.org/books**.

Enter Discount Code **MRSMEMBER** at checkout to apply the MRS Member discount for these and all Cambridge science/engineering books and proceedings.
Not an MRS Member? Join today at **www.mrs.org/join.**

MRS MATERIALS RESEARCH SOCIETY®
CAMBRIDGE UNIVERSITY PRESS

https://doi.org/10.1557/mrs.2016.211 Published online by Cambridge University Press